# Controlling quantum interference in tetraphenyl-aza-BODIPYs

Alaa A. Al-Jobory[a,b] and Ali K. Ismael[a*,c]

This study presents systematic theoretical investigations employing an ab initio DFT approach combined with analysis of heuristic tight-binding models. We examine the effect of using conjugated and non-conjugated bridge on the electrical transport of tetraphenyl-aza-BODIPY derivatives. This work demonstrates that, substitution a conjugated bridging atom by non-conjugated one, causes the electrical conductance to switch from constructive quantum interference CQI to destructive DQI (on/off). This demonstration of switching behaviour means that if molecules with alternating structures (i.e., non-/conjugated), can be deposited on a metal surface, then they form a basis for enhancing the thermovoltage in nanoscale thermoelectric nanotechnology devices.

*To whom correspondence should be addressed. e-mail: k.ismael@lancaster.ac.uk

## 1 Introduction

Interference is occurring all waves such as sound, gravitational, electromagnetic and water waves. This phenomenon exists when two waves are superposed to form a combined wave. The two waves can either superpose destructively or constructively, the former is resulting in a small combined amplitude, whereas the latter is resulting in a large combined amplitude. The term "*quantum interference (QI)*" is first used to describe interference of de Broglie waves.[1]

Quantum interference is also taking place in molecular electronics as long as the energy of an electron passing through a molecule is not changed as it moves via the molecule. This indicts that the phase of the wave function is not changed and this called "*phase coherent transport*".[2]

QI provides a method to modulate the charge transfer through nanoscale devices and materials at a molecular scale level, which is of great influence for the design of future high-efficiency switchable devices.[3-8] In recent years, many studies revealed that extended π systems of multi-pathed molecules present QI effects.[9-16] To illustrate that, molecular structures displaying constructive quantum interference (CQI) in their π systems were identified to have boosted their electrical conductance, contrary to those showing destructive quantum interference (DQI), had relatively low conductance.[17-19] It should be noted that, for the latter, the measured conductances were still higher than the theoretical predictions as consequence of the existence of adventitious σ transport channels,[20-24]which diminish the impact of the destructive interference in pi-systems.

Paddon-Row and co-workers[25] investigated how to electrochemically control QI in a single anthraquinone-based norbornylogous bridge molecule. AQ molecules have similar cores to our studied molecules. However, AQs are cross-conjugated which make them easier to electrochemically control while ours are conjugated and non-conjugated. This group[26] also explored the electrochemical gating for the same family of molecules using the STM break-junction technique. In 2018,[27] the AQ molecules were attached to a thioacetate anchors from both sides(symmetric), SAc and phenyl ring (asymmetric), and investigated the QI effect on the charge transport.

To achieve a highly insulating molecular bridge, it is pivotal to develop strategies that lead to introducing DQI into conjugated systems.[28] The conjugated and non-conjugated bridge formed by an atom or group has been intensively used as a linker to combine two molecular building blocks.[8, 29, 30]

To accomplish QI in molecular scale structures, numerous of theoretical and experimental studies have suggested the

introduction of gauche configuration in the covalent backbone by permethylation on the covalently bonded atoms,[23, 31, 32] or constructing dual and even triple channels in σ-conjugated alkane or silane systems.[33] However, both the permethylation and silylation require intensive synthetic efforts with longer molecular lengths.[34, 35] alternatively, aza-BODIPYs are potential candidates for controlling QI effects at a molecular scale level.

In the current work, we investigate the electric properties of conjugated and non-conjugated molecular structures of tetraphenyl-aza-BODIPYs with 4 thiomethyl terminal end groups. Fig. 1 below, illustrates the anatomy of two aza-BODIPYs. Each of which consists of two highly conductive pathways and linked by a bridge. This bridge could be conductive if it is conjugated, means the two parallel pathways connected by a conjugated N atom and $BF_2^+$ group as shown in Fig. 1a. In contrast, the bridge is non-conductive if the conjugation is breaks off, means the two parallel pathways connected by non-conjugated groups such as $BF_2^+$ (see Fig. 1b).

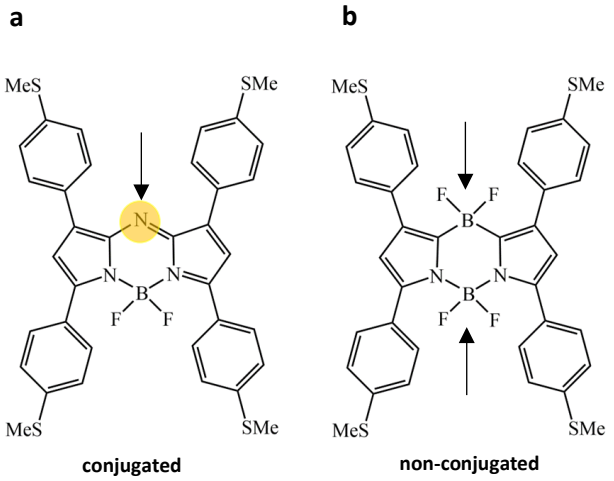


**Figure 1.** Examples of aza-BODIPY-based molecules with four thiomethyl terminal groups *SMe*. (**a**) *conductive-bridge*, conjugated tetraphenyl-aza-BODIPY. (**b**) *non-conductive-bridge*, non-conjugated tetraphenyl-aza-BODIPY. (Note: (a) conjugated by the nitrogen atom, while (b), non-conjugated by $2BF_2^+$ groups).

In our previous work[36], three conjugated aza derivatives explored intensively both theoretically and experimentally. Herein, we shall restrict this research on the comparison between conjugated and non-conjugated aza-BODIPYs as shown in Fig.1. Both conjugated and non-conjugated motifs are rigid, flat, and highly conjugated molecules consisting of two conjugated parallel paths. The two aza molecules differ by the bridging atom (shaded in orange, Fig. 1a), which is N or $BF_2^+$ for the conjugated and non-conjugated (panels a and b of Fig.1). Both molecules possess 4 terminal end groups and in Au/aza-based/Au junction there are several possible geometries (see ref.[36]). However, here we shall focus on the two likely contact orientations: straight (along the pathway, **1-3**) and diagonal (via the central heterocycle, **1-7**) ones as shown in Fig. 2a.

Following, we will examine the conjugated and non-conjugated aza-BODIPYs. Gold electrodes are bound to the terminal groups in two different orientations (i.e., straight and diagonal), for the conjugated molecule, and diagonal orientation for the non-conjugated (Note: for clarity, only the cores of aza-BODIPYs are shown in Fig. 2a).

## 2 Methods

To calculate the electrical transport through the conjugated and non-conjugated aza-BODIPYs. We began by modelling the terminal SMe-Au binding, and then relaxed each compound in the presence of fixed leads. Using the density functional code SIESTA[37] (for more detail see geometry of isolated aza-BODIPYs in the SI) the optimum geometries of isolated aza-BODIPY derivatives were obtained by relaxing the molecules until all forces on the atoms were less than 0.05 eV / Å (see Supplementary Fig. S1). We used a double-zeta plus polarization orbital basis set, norm-conserving pseudopotentials, the local density approximation (LDA) exchange correlation functional, and to define the real space grid, an energy cutoff of 250 Rydbergs. We also computed results using GGA and found that the resulting transmission functions were comparable[38, 39] with those obtained using LDA. To simulate the likely contact configuration during a break-junction experiment, we employed leads constructed from 6 layers of Au (111), each containing 30 gold atoms and further terminated with a pyramid of gold atoms. After relaxing each molecular junction in different orientations, we calculated the electrical conductance using the Gollum quantum transport code,[40] (for more details see section 4 of the SI).

## 3 Results and discussion

The transport properties of aza-BODIPY junctions involving 4 thiomethyl anchor groups were modelled using a combination of density functional theory and quantum transport theory. To have a good understanding of electronic properties, the frontier orbital of studied molecules: highest occupied molecular orbitals (HOMO) and

lowest unoccupied orbitals (LUMO) along with their energies are investigated and it should be noted that the orbitals product rule[41] do not apply on aza-BODIPY molecules due to the degeneracy in HOMOs and HOMO-1s orbitals, as shown in Supplementary Figs. S2-S3. The optimal binding distance between the electrodes and the thiomethyl anchor groups were obtained by calculating their binding energies as a function of distance (*Au- SMe*), the covalent bond distance is found to be 2.9 Å, and the actual bending energy approximately 0.3 eV, as illustrated in Supplementary Fig. S4 (for more detail see the binding energy simulations in the SI).

As a first step, we investigated transport through these aza-BODIPY derivatives in *Au-Au* junctions. Thiomethyl anchor group illustrates a unique type of transport. In other words, a LUMO-dominated transport, hinting that the 4-*SMe* groups move the LUMO closest to the Fermi energy as shown in Supplementary Fig. S6, (for more detail see DFT simulations in the SI).

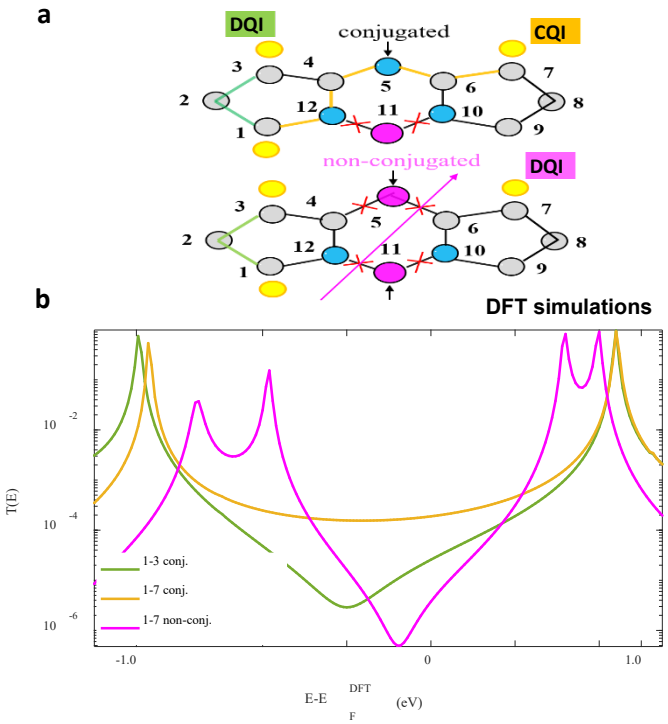


**Figure 2.** (**a**) Lattice representation of aza-BODIPYs with either straight **1-3** or diagonal **1-7** contact (for clarity only the core units are shown, yellow circles represent Au electrodes). Conjugated and non-conjugated lattices when the two 5-membered rings are bridged by the nitrogen/boron atoms (blue and purple circles on site 5, for comparison see the core units of Fig. 1). (**b**) Zero bias transmission coefficients *T(E),* obtained from density functional theory (DFT), in three different possible junctions (see top panel). Conjugated lattice: straight (**1-3** short path to convey electrons from one electrode to another, green-line), and diagonal (**1-7** long path, orange-line). Non-conjugated lattice: diagonal (long path, purple-line).

To aid the discussion only the central units (cores), of aza-BODIPYs are shown in Fig. 2a, and libelled **1-12.** Despite the fact that Fig. 2b, results show that the transmission coefficients near the DFT-predicted Fermi energy for the conjugated and non-conjugated aza-BODIPYs are LUMO-dominated in three orientations. However, the conductance differs by the trend and magnitude. As described above (Fig. 2a), the three orientations corresponding to different connectivities **1-3** and **1-7**, to gold electrodes. Connectivity **1-3** produces a low conductance ($G$), for the conjugated motif, whereas **1-7** yields a high $G$ of the same motif (conjugated), as shown by the green and orange transmission coefficient curves in Fig. 2b. This behaviour (i.e., high/low $G$), in the HOMO-LUMO gap can be explained by the quantum interference QI effect that electrons undergo when pass from one electrode to another through the aza motif. QI will be explored in more detail in next section.

Moving to the non-conjugated motif by replacing the bridging atom N by $BF_2^+$ group and recalculate the transmission coefficient $T(E)$, via **1-7** connectivity. It is clearly shown by the purple curve the conductance declines again. The switching behaviour from high to low (compare orange- versus purple-curve), occurs because the conjugation in the conductance channel was broken (see the purple arrow in Fig. 2a). It should be noted that, although the **1-7** connectivity yields a low conductance in both conjugated and non-conjugated motifs, however, the $G$ is much lower through the non-conjugated one at the DFT-predicted Fermi energy $E - E_F^{DFT}$= 0 eV.

## Quantum interference QI

After the DFT discussion above, in this section, we shall employ a tight-binding model (TBM), to probe the connectivity dependence of transport through the aza lattice of Fig. 3a, (see section 5.2 in the SI). For the lattice in Fig. 3a, if all the sites were identical, then the simplest model would be obtained by setting all $\varepsilon_j$=0 (which defines the zero of energy) and all nearest neighbour couplings equal to -1, which sets the energy scale. The obtained Hamiltonian is a simple connectivity table, whose entries $H_{ij}$ are equal to -1 when two atoms i and j are neighbours and are zero otherwise.

Despite its simplicity, Huckel's model (TBM), is found to describe the connectivity dependence of the electrical conductance of molecules with polyaromatic hydrocarbon cores.[42, 43] In this model, there are some inequivalent atoms, coloured light blue (nitrogens), purple (boron) and grey (carbons), and thus we assign these different site energies, denoted **1-12** ($\varepsilon_C$=$\varepsilon_N$=$\varepsilon_B$=0).

When semi-infinite one-dimensional crystalline leads are coupled to sites **1** and **3**, the $T(E)$ is shown as the green curve in Fig. 3b, which clearly exhibits a destructive quantum interference (DQI), dip. On the other hand, when crystalline leads are linked to sites **1** and **7**, the orange curve is produced and possesses no DQI signature (i.e., dip), these results for the conjugated lattice (sites **5, 10, 12** are nitrogens, and **11** is boron, $\varepsilon_N$=0, $\varepsilon_B$=**4**), for more detail see TMB simulations in the SI.

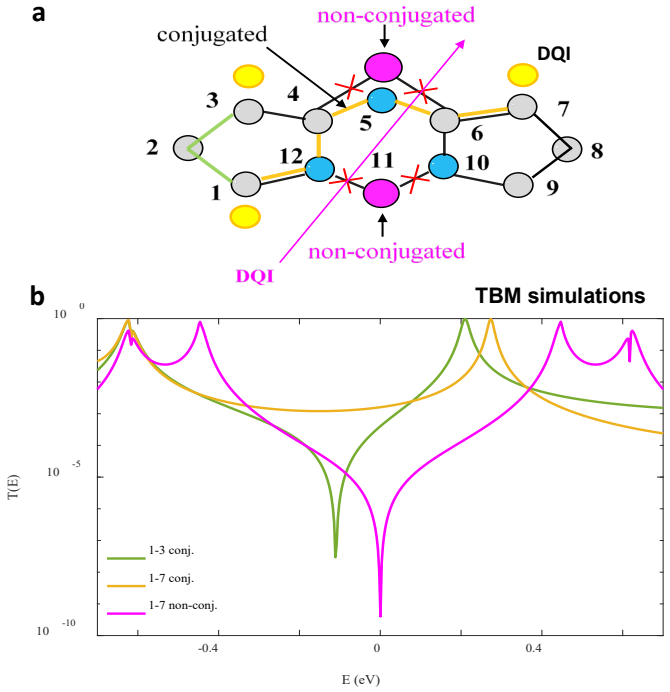


**Figure 3.** (**a**): Lattice representation of an aza-BODIPY core with either straight **1-3** or diagonal **1-7** contact (yellow circles represent Au electrodes). Conjugated and non-conjugated lattices when the two 5-membered rings are bridged by the nitrogen/boron atoms (blue and purple on site **5**, see the core units of Fig. 1). (**b**): Core transmission coefficients, obtained from the tight binding model (TBM), in three different possible junctions (see top panel). Conjugated lattice: straight (**1-3** short path to convey electrons from one electrode to another, green-line), and diagonal (long path, orange-line). Non-conjugated lattice: diagonal (**1-7** long path, purple-line). Note: TBM detail, the coupling parameter γ=-1 and on energy sites of carbon, nitrogen and boron are $\varepsilon_C$=0, $\varepsilon_N$=0, $\varepsilon_B$=4.

Transitioning to the non-conjugated lattice (sites **11, 12** are nitrogens, and **5, 11** are borons, $\varepsilon_N$=0, $\varepsilon_B$=4). Here, we restrict the investigations on **1-7** only as it produces the lowest conductance in the DFT simulations $(G_{\mathbf{1-7}})_{\text{conj.}} > (G_{\mathbf{1-3}})_{\text{conj.}} > (G_{\mathbf{1-7}})_{\text{non-conj.}}$, as illustrated in Fig. 2b. Again, the TBM for this non-conjugated connectivity yields the lowest $G$ as signifies by a sharp dip at $E$= 0. Nevertheless, that both conjugated and non-conjugated motifs (more precisely, **1-3** and **1-7** connectivities respectively), exhibit a destructive quantum interference, however, the DQI of the conjugated motif is significantly higher than the non-conjugated one at the Fermi level ($E$= 0). This can be elucidated as in the case of the conjugated motif there is still a conductive pathway between the two 5-membered rings through the bridging atom (nitrogen). In contrast, this pathway is no longer conductive when the bridging site is un-conjugated by difluoroboryl ($BF_2^+$ group), and this explains why $G$ is much lower with a sharp DQI dip.

TBM results are in qualitative agreement with the DFT transmission coefficient plots as shown in Supplementary Fig. S9 of the SI. Both TBM and DFT approaches demonstrate that in the presence of the **1-7** connectivity, there is no signature of a DQI for the conjugated motif. However, the same connectivity switches from CQI to DQI when the bridging atom substitutes by a non-conjugated group. This research demonstrates that the conductance through two parallel paths connect to each other through a bridge is sensitive to the nature of the bridging linker. It suggests a high $G$ for conjugated linkers dissimilar to non-conjugated ones. The high and low $G$ attributes to the QI effect that occurs in multi-pathed molecular structures.[12, 44-47]

## 4 Conclusions

In conclusion, through a systematic study, we have demonstrated that transport via aza-BODIPY-based molecular wires involving one bridging atom switch the conductance from high to low (on/off), by substituting the bridging atom from conjugated to non-conjugated. Tetraphenyl-aza-BODIPY molecules with four thiomethyl terminal groups compose strong contacts with gold surface within the BJ-STM. Based on that, these molecules can form different junction geometries corresponding to different connectivities to Au electrodes. **1-3** and **1-7** connectivities of the same conjugated motif switches the transport from DQI to CQI, such a feature is of great interest in designing high performance thermoelectric devices. DFT and TBM simulations have shown that the electrical transport of aza-BODIPY derivatives can be systematically tuned and boosted by varying the bridging atom and contact points. Furthermore, this work opens new ideas for designing new nanotechnology devices with potential practical applications.

## Conflicts of interest

There are no conflicts to declare.

## Acknowledgements

This work was supported by the Leverhulme Trust for Early Career Fellowship ECF-2020-638. This work was additionally funded by the European Commission FET Open projects 767187-QuIET and 766853-EFINED. A.A. is grateful for financial assistance from Anbar University (Iraq). A.K.I is grateful for financial assistance from Tikrit University (Iraq), and the Iraqi Ministry of Higher Education (SL-20).

## Author contributions

A.K.I originally conceived the concept, calculations were carried out by A.A. Both authors have given approval to the final version of the manuscript. Both authors provided essential contributions to interpreting the data reported in this manuscript. A.K.I coordinated the writing of the manuscript with input from A.A.

## References

1. L. De Broglie, *Ondes et mouvements*, Gauthier-Villars, 1926.
2. C. J. Lambert, *Quantum Transport in Nanostructures and Molecules*, IOP Publishing, 2021.
3. T. A. Su, M. Neupane, M. L. Steigerwald, L. Venkataraman and C. Nuckolls, *Nat. Rev. Mater.*, 2016, **1**, 16002.
4. L. A. Wilkinson, T. L. Bennett, I. M. Grace, J. Hamill, X. Wang, S. Au-Yong, A. Ismael, S. P. Jarvis, S. Hou and T. Albrecht, *Chemical Science*, 2022, **13**, 8380-8387.
5. N. J. Tao, *Nat Nanotechnol*, 2006, **1**, 173-181.
6. M. Alshammari, A. A. Al-Jobory, T. Alotaibi, C. J. Lambert and A. Ismael, *Nanoscale Advances*, 2022, **4**, 4635-4638.
7. M. L. Perrin, E. Burzurí and H. S. van der Zant, *Chemical Society Reviews*, 2015, **44**, 902-919.
8. N. Xin, J. X. Guan, C. G. Zhou, X. J. N. Chen, C. H. Gu, Y. Li, M. A. Ratner, A. Nitzan, J. F. Stoddart and X. F. Guo, *Nat Rev Phys*, 2019, **1**, 211-230.
9. M. Koole, J. M. Thijssen, H. Valkenier, J. C. Hummelen and H. S. Van Der Zant, *Nano Lett.*, 2015, **15**, 5569-5573.
10. A. Alshehab and A. K. Ismael, *RSC Advances*, 2023, **13**, 5869-5873.
11. C. Joachim, *Nat Nanotechnol*, 2012, **7**, 620-621.
12. T. L. Bennett, M. Alshammari, S. Au-Yong, A. Almutlg, X. Wang, L. A. Wilkinson, T. Albrecht, S. P. Jarvis, L. F. Cohen and A. Ismael, *Chem. Sci.*, 2022, **13**, 5176-5185.
13. T. Hansen and G. C. Solomon, *The Journal of Physical Chemistry C*, 2016, **120**, 6295-6301.
14. X. Wang, A. Ismael, A. Almutlg, M. Alshammari, A. Al-Jobory, A. Alshehab, T. L. Bennett, L. A. Wilkinson, L. F. Cohen and N. J. Long, *Chemical science*, 2021, **12**, 5230-5235.
15. A. Borges, J. Xia, S. H. Liu, L. Venkataraman and G. C. Solomon, *Nano Lett.*, 2017, **17**, 4436-4442.
16. S.-H. Ke, W. Yang and H. U. Baranger, *Nano Lett.*, 2008, **8**, 3257-3261.
17. H. Vazquez, R. Skouta, S. Schneebeli, M. Kamenetska, R. Breslow, L. Venkataraman and M. Hybertsen, *Nature Nanotechnology*, 2012, **7**, 663.
18. H. Chen, H. Zheng, C. Hu, K. Cai, Y. Jiao, L. Zhang, F. Jiang, I. Roy, Y. Qiu and D. Shen, *Matter-Us*, 2020, **2**, 378-389.
19. D. Miguel, L. Alvarez de Cienfuegos, A. Martín-Lasanta, S. P. Morcillo, L. A. Zotti, E. Leary, M. Bürkle, Y. Asai, R. Jurado and D. J. Cárdenas, *Journal of the American Chemical Society*, 2015, **137**, 13818-13826.
20. J. M. Hamill, A. Ismael, A. Al-Jobory, T. L. Bennett, M. Alshahrani, X. Wang, M. Akers-Douglas, L. A. Wilkinson, B. J. Robinson and N. J. Long, *arXiv preprint arXiv:2210.17232*, 2022.
21. A. Borges, E.-D. Fung, F. Ng, L. Venkataraman and G. C. Solomon, *The journal of physical chemistry letters*, 2016, **7**, 4825-4829.
22. S.-X. Liu, A. K. Ismael, A. Al-Jobory and C. J. Lambert, *Accounts of chemical research*, 2023, 4193-4201.
23. M. H. Garner and G. C. Solomon, *The Journal of Physical Chemistry Letters*, 2020, **11**, 7400-7406.
24. M. K. Al-Khaykanee, A. K. Ismael, I. Grace and C. J. Lambert, *Rsc Advances*, 2018, **8**, 24711-24715.
25. N. Darwish, I. Díez-Pérez, P. Da Silva, N. Tao, J. J. Gooding and M. N. Paddon-Row, *Angewandte Chemie*, 2012, **124**, 3257-3260.
26. N. Darwish, I. Diez-Perez, S. Guo, N. Tao, J. J. Gooding and M. N. Paddon-Row, *The Journal of Physical Chemistry C*, 2012, **116**, 21093-21097.
27. C. M. Guédon, H. Valkenier, T. Markussen, K. S. Thygesen, J. C. Hummelen and S. J. Van Der Molen, *Nature nanotechnology*, 2012, **7**, 305-309.
28. M. Carlotti, S. Soni, S. Kumar, Y. Ai, E. Sauter, M. Zharnikov and R. C. Chiechi, *Angew Chem Int Edit*, 2018, **57**, 15681-15685.
29. C. Jia, A. Migliore, N. Xin, S. Huang, J. Wang, Q. Yang, S. Wang, H. Chen, D. Wang and B. Feng, *Science*, 2016, **352**, 1443-1445.
30. R. H. Goldsmith, J. Vura-Weis, A. M. Scott, S. Borkar, A. Sen, M. A. Ratner and M. R. Wasielewski, *Journal of the American Chemical Society*, 2008, **130**, 7659-7669.
31. B. P. Paulson, L. A. Curtiss, B. Bal, G. L. Closs and J. R. Miller, *Journal of the American Chemical Society*, 1996, **118**, 378-387.
32. M. Alshammari, T. Alotaibi, M. Altoaibi and A. K. Ismael, *Energies*, 2023, **16**, 4342.
33. H. Li, M. H. Garner, T. A. Su, A. Jensen, M. S. Inkpen, M. L. Steigerwald, L. Venkataraman, G. C. Solomon and C. Nuckolls, *Journal of the American Chemical Society*, 2017, **139**, 10212-10215.
34. E. M. Press, E. A. Marro, S. K. Surampudi, M. A. Siegler, J. A. Tang and R. S. Klausen, *Angew. Chem. Int. Ed.*, 2017, **56**, 568-572.
35. A. Wallner, R. Emanuelsson, J. Baumgartner, C. Marschner and H. Ottosson, *Organometallics*, 2013, **32**, 396-405.
36. A. Markin, A. K. Ismael, R. J. Davidson, D. C. Milan, R. J. Nichols, S. J. Higgins, C. J. Lambert, Y.-T. Hsu, D. S. Yufit and

A. Beeby, *The Journal of Physical Chemistry C*, 2020, **124**, 6479-6485.
37. J. M. Soler, E. Artacho, J. D. Gale, A. García, J. Junquera, P. Ordejón and D. J. J. o. P. C. M. Sánchez-Portal, *Journal of Physics: Condensed Matter*, 2002, **14**, 2745.
38. A. K. Ismael, A. Al-Jobory, I. Grace and C. J. Lambert, *The Journal of chemical physics*, 2017, **146**, 064704.
39. A. K. Ismael, I. Grace and C. J. Lambert, *Nanoscale*, 2015, **7**, 17338-17342.
40. J. Ferrer, C. J. Lambert, V. M. García-Suárez, D. Z. Manrique, D. Visontai, L. Oroszlany, R. Rodríguez-Ferradás, I. Grace, S. Bailey and K. Gillemot, *New Journal of Physics*, 2014, **16**, 093029.
41. C. J. Lambert and S. X. Liu, *Chemistry–A European Journal*, 2018, **24**, 4193-4201.
42. M. T. González, A. K. Ismael, M. Garcia-Iglesias, E. Leary, G. Rubio-Bollinger, I. Grace, D. Gonzalez-Rodriguez, T. Torres, C. J. Lambert and N. Agrait, *The Journal of Physical Chemistry C*, 2021, **125**, 15035-15043.
43. C. J. Lambert, *Chemical Society Reviews*, 2015, **44**, 875-888.
44. A. K. Ismael, I. Grace and C. J. Lambert, *Phys. Chem. Chem. Phys.*, 2017, **19**, 6416-6421.
45. L. Herrer, A. Ismael, S. Martin, D. C. Milan, J. L. Serrano, R. J. Nichols, C. Lambert and P. Cea, *Nanoscale*, 2019, **11**, 15871-15880.
46. A. K. Ismael and C. J. Lambert, *J. Mater. Chem. C*, 2019, **7**, 6578-6581.
47. J. Ye, A. Al-Jobory, Q.-C. Zhang, W. Cao, A. Alshehab, K. Qu, T. Alotaibi, H. Chen, J. Liu and A. K. Ismael, *Sci. China Chem*, 2022, **65**, 1822–1828.